An Unsupervised Learning Method for Indirect Bridge Structural Health Monitoring

Andres Calderon Hurtado[1(✉)], Mehrisadat Makki Alamdari[1],
E. Atroshchenko[1], Kai-Chun Chang[2], and Chul-Woo Kim[2]

[1] Center for Infrastructure Engineering and Safety, School of Civil and Environmental Engineering, University of New South Wales, Sydney, NSW 2052, Australia
a.calderonhurtado@student.unsw.edu.au
[2] Department of Civil & Earth Resources Engineering,
Graduate School of Engineering, Kyoto University, Kyoto 615-8540, Japan

Abstract. Over the last decade, the use of drive-by inspection technology for bridge damage assessment has been widely studied by scholars. It consists of identifying bridge damage from the response of an instrumented sensing vehicle. Most current methods are based on identifying bridge properties and supervised learning techniques. However, these approaches require data from the bridge at its different states (i.e., healthy and damaged conditions), which is not always available. Hence, this study proposes a fully unsupervised deep learning-based methodology for bridge structural health monitoring (SHM) based on the time-frequency domain analysis of the acceleration signal recorded by a two-axle vehicle. A convolutional variational autoencoders (CVAE) algorithm is trained only with the Continuous Wavelet Transform (CWT) of vehicle acceleration response while passing over a bridge at its benchmark state. The damage index is defined from the measured error between the original and the reconstructed CWT images. During testing, the error between the original and the reconstructed CWT is compared with the damage index from the benchmark state to classify the new samples as healthy or damaged. The method is tested on a numerical vehicle-bridge interaction (VBI) model using finite elements. Different damage severities and the effect of road roughness are studied.

Keywords: Convolutional variational autoencoder · Deep learning · Indirect SHM · Bridge monitoring · Damage assessment

1 Introduction

Current worldwide society depends extensively on large infrastructures, especially on bridges. As Lin and Yoda in [1] mentioned in their work, bridges serve as "lifelines" in social infrastructure since they constitute a major part of the contemporary highway and railway systems. Likewise, bridges are susceptible to continuous changes in the conditions they are subjected to (e.g. load history, environmental and hazardous events, material degradation, malfunctioning

connecting elements) over their service life [2], which has entailed a new concern over the structural health of bridges in the world.

SHM systems can be classified as *direct* or *indirect*, based on the information used to assess the damage on the structure. Direct SHM systems involve installing multiple sensors of different kinds at specific structure locations, to continuously measure the structure's response, which is used to assess the structure's health condition [3]. However, the installation and maintenance process of direct SHM systems is costly, labor-intensive, complex, and unsafe [4]. On the other hand, indirect SHM systems based on drive-by inspection are more economical and safer [3]. They consist of sensing the target bridge with an instrumented moving vehicle which is capable of measuring the combined response of itself and the bridge, from which damage can be assessed [5,6].

Additionally, both direct and indirect SHM techniques can be classified in physics-based approaches and data-driven approaches. The first one consists of identifying damage from the variation of the dynamical properties of the bridge, including natural frequencies and mode shapes [7–11]. However, such methodologies require previous knowledge of the structure, which is only sometimes available. The latter focuses primarily on data analysis of the recorded responses to assess the structural health [2,3,5,12–15].

In recent years, the interest in machine learning and deep learning approaches for damage identification in indirect SHM has risen [14]. Nonetheless, few studies have cover the bridge damage assessment problem from an unsupervised perspective [16]. This work presents a data-driven indirect SHM methodology for bridge damage assessment based on drive-by inspection using an unsupervised learning technique, which only utilizes information learned from the healthy state of the bridge to determine the structure's condition.

The structure of this paper is the following: Sect. 2 presents the details of the VBI model adopted in the numerical simulations. Section 3 introduces the numerical dataset. The unsupervised damage assessment framework is presented in Sect. 4, and the results discussion is presented in Sect. 5. Lastly, Sect. 6 presents conclusions and recommendations for future work.

2   Vehicle Bridge Interaction Model

2.1   VBI Governing Equations

This section presents the dynamic coupling equations describing the interaction between a bridge and a vehicle traveling over it. The vehicle used in this work is a half-car model consisting of two degrees of freedom (DOF) (i.e., bounce and pitch respectively).

Figure 1 shows the half-car model associated with the two DOF, bouncing vibration, $z_v(t)$, and pitching vibration, $\theta_v(t)$, from which the axles vibration is measurable. The vehicle is described by eight parameters as follows: k_{v_i} and c_{v_i} correspond to the i-th axle stiffness and damping respectively, where $i = 1, 2$. m_v and I_v represent the mass and moment of inertia of the vehicle respectively. d_i corresponds to the distance from the center of gravity (C.G.) to the i-th
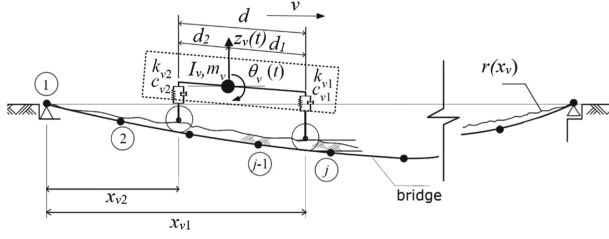
Fig. 1. VBI illustration of model used in numerical simulations

axle. A constant speed, v, of the vehicle while moving over the bridge, and no separation between the tire and the road is assumed.

The bridge is modeled as a simply supported Euler-Bernoulli beam with stochastic road profile $r(x_{v_i})$, where x_{v_i} represents the location of the i-th axle. The governing equations of the sensing vehicle are described in Eqs. 1 and 2, where $\{\mathbf{Z}_b(t)\} = \{Z_{b,1}(t), Z_{b,2}(t), \cdots, Z_{b,i}(t), \cdots, Z_{b,n}(t)\}$ is the vector of the nodal coordinates of the bridge system and, n is the number of DOF for the bridge. $\{\boldsymbol{\iota_b}(x_{v_i})\}$ is a vector containing shape functions to interpolate the displacement of the bridge system observed at the contact point of i-th axle, i.e., x_{v_i}. Overdot and prime symbols represent the derivatives with respect to time and space, respectively.

$$
\begin{aligned}
m_v \ddot{z}_v(t) + c_{v_1}[\dot{z}_v(t) + d_1\dot{\theta}_v(t) - \{\boldsymbol{\iota_b}(x_{v_1})\}^T\{\dot{\mathbf{Z}}_b(t)\} + vr'(x_{v_1})] \\
+ c_{v_2}[\dot{z}_v(t) - d_2\dot{\theta}_v(t) - \{\boldsymbol{\iota_b}(x_{v_2})\}^T\{\dot{\mathbf{Z}}_b(t)\} + vr'(x_{v_2})] \\
+ k_{v_1}[z(t) + d_1\theta_v(t) - \{\boldsymbol{\iota_b}(x_{v_1})\}^T\{\mathbf{Z}_b(t)\} + r(x_{v_1})] \\
+ k_{v_2}[z_v(t) - d_2\theta_v(t) - \{\boldsymbol{\iota_b}(x_{v_2})\}^T\{\mathbf{Z}_b(t)\} + r(x_{v_2})] = 0
\end{aligned}
\tag{1}
$$

$$
\begin{aligned}
I_v\ddot{\theta}_v(t) + d_1\big(c_{v_1}[\dot{z}_v(t) + d_1\dot{\theta}_v(t) - \{\boldsymbol{\iota_b}(x_{v_1})\}^T\{\dot{\mathbf{Z}}_b(t)\} + vr'(x_{v_1})] + \\
k_{v_1}[z_v(t) + d_1\theta_v(t) - \{\boldsymbol{\iota_b}(x_{v_1})\}^T\{\mathbf{Z}_b(t)\} + r(x_{v_1})]\big) \\
- d_2\big([c_{v_2}[\dot{z}_v(t) - d_2\dot{\theta}_v(t) - \{\boldsymbol{\iota_b}(x_{v_2})\}^T\{\dot{\mathbf{Z}}_b(t)\} + vr'(x_{v_2})] + \\
k_{v_2}[z_v(t) - d_2\theta_v(t) - \{\boldsymbol{\iota_b}(x_{v_2})\}^T\{\mathbf{Z}_b(t)\} + r(x_{v_2})]\big) = 0
\end{aligned}
\tag{2}
$$

The equilibrium equations of the system, using a finite element model (FEM), are presented in Eqs. 3, 4 and 5,

$$
[\mathbf{M_b}]\{\ddot{\mathbf{Z}}_b(t)\} + [\mathbf{C_b}]\{\dot{\mathbf{Z}}_b(t)\} +
$$
$$
[\mathbf{K_b}]\{\mathbf{Z}_b(t)\} + \{\boldsymbol{\iota_b}(x_{v_1})\}R_1(t) + \{\boldsymbol{\iota_b}(x_{v_2})\}R_2(t) = 0
\tag{3}
$$

$$
R_1(t) = -c_{v_1}[\dot{z}_v(t) - \{\boldsymbol{\iota_b}(x_{v_1})\}^T\{\dot{\mathbf{Z}}_b(t)\} + vr'(x_{v_1})]
$$
$$
- k_{v_1}[z_v(t) - \{\boldsymbol{\iota_b}(x_{v_1})\}^T\{\mathbf{Z}_b(t)\} + r(x_{v_1})] + \left(\frac{d_2}{d}\right)m_vg
\tag{4}
$$

$$
R_2(t) = -c_{v_2}[\dot{z}_v(t) - \{\boldsymbol{\iota_b}(x_{v_2})\}^T\{\dot{\mathbf{Z}}_b(t)\} + vr'(x_{v_2})]
$$
$$
- k_{v_2}[z_v(t) - \{\boldsymbol{\iota_b}(x_{v_2})\}^T\{\mathbf{Z}_b(t)\} + r(x_{v_1})] + \left(\frac{d_1}{d}\right)m_vg
\tag{5}
$$

where, $R_1(t)$ and $R_2(t)$ are, respectively, the contact forces at axle locations, x_{v_1} and x_{v_2}, and g is the gravitational acceleration. By combining Eqs. 1, 2, and 3, the governing coupled equation for the vehicle-bridge interaction system can be obtained [17]. The coupled dynamic equation is then solved using the Newmark-Beta method.

2.2 Damaged Beam Model

The damage in the beam is simulated using the simplified crack model presented by Sinha et al. [18]. The model consists of reducing the beam stiffness linearly over a length of $1.5h$ at each side of the crack. Equation 6 represents the flexural stiffness variation, $EI_e(\zeta)$, in the vicinity of the crack [18]

$$EI_e(\zeta) = \begin{cases} EI_0 - E(I_0 - I_c)\dfrac{\zeta - \zeta_1}{\zeta_c - \zeta_1} & \text{if } \zeta_1 \leq \zeta \leq \zeta_c \\[2ex] EI_0 - E(I_0 - I_c)\dfrac{\zeta_2 - \zeta}{\zeta_2 - \zeta_c} & \text{if } \zeta_c \leq \zeta \leq \zeta_2 \end{cases} \tag{6}$$

where E is the Young's modulus of the beam, I_o is the undamaged section's second moment of inertia, ζ is the spatial coordinate and ζ_c is the crack location. ζ_1 and ζ_2 are the positions on the left and right sides of the crack, respectively, where the stiffness reduction begins. I_c is the cracked section's second moment of the inertia given by $I_c = b(h - h_c)^3/12$, where b is the beam width, h is the beam height, and h_c is the crack depth.

2.3 Road Roughness Profile

The stochastic road roughness profile $r(x)$ is modeled following the procedure presented in ISO8608 [19]. The roughness type is described by the Power Spectral Density (PSD) function, $G_d(n) = G_d(n_0)(n/n_0)^{-w}$, where, n is the spatial frequency per meter, $w = 2$, $n_0 = 0.1$ cycle/m, and the functional value $G_d(n_0)$ is determined by the roughness type in ISO 8608 (i.e., type A-D) [19]. The amplitude of the road profile is given as $\eta = \sqrt{2G_d(n)\Delta n}$, where Δn is the sampling interval of the spatial frequency. The road roughness profile is given in Eq. 7

$$r(x) = \sum \eta_i \cos(n_i x + \theta_i) \tag{7}$$

where n_i is the i-th spatial frequency, and η_i and θ_i denote the amplitude and the random phase angle, respectively, of the i-th cosine function. The phase angle follows a uniform distribution in the interval of $[0, 2\pi)$, the sampling interval Δn for the spatial frequency is taken as 0.04 cycle/m, and the range of spatial frequency n is 1-100 cycle/m [19]. It is important to mention that a road profile type A is used throughout this work.

3   Numerical Case Study

3.1   Bridge and Vehicle Properties

The bridge model is based on the studies performed by McGetrick et al. in [12,20], and its properties are presented in Table 1.

Table 1. A summary of bridge's physical properties.

Property	Value	Property	Value
Span length, L	25 m	Cross section area, A	16.68 m^2
Young's modulus, E	3.5×10^{10} N/m^2	Second moment of inertia, I_o	1.39 m^4
Mass per unit length, μ	$18,358$ kg/m	Damping ratio, ξ	3%
First three natural frequencies, f_b		$4.09Hz$, $16.36Hz$ and $36.8Hz$	

Four different states of the bridge, i.e., BC0, and BCM1:BCM3, are created, where BC0 refers to the intact bridge, and BCM1:BCM3 refer to a damaged bridge. Damage is induced at mid-span of the beam, using the model presented in Sect. 2.2. Damage conditions BCM1 to BCM3 correspond to crack depth to beam height ratios of 10%, 20%, and 30%, respectively. Additionally, BCM1, BCM2 and BCM3 produce a reduction in the first natural frequency of 1.9%, 4.16% and 6.85% respectively.

The sensing vehicle properties are based on the relevant reference studies in [12,20]. Table 2 shows the vehicle characteristics. The vehicle is assumed to travel over the bridge at a constant speed in each pass. The speed at each pass is defined randomly by a normal distribution with 2 m/s mean value and 0.2 m/s standard deviation.

Table 2. A summary of vehicle physical properties.

Property	Value	Property	Value
Vehicle mass, m_v	16,200 kg	Axle damping, c_v	1×10^4 Ns/m
Vehicle inertia, I_v	93,234 $kg \cdot m^2$	C.G to front axle distance, d_1	2.375 m
Axle stiffness, k_v	4×10^5 N/m	C.G to rear axle distance, d_2	2.375 m
Bouncing natural frequency, f_z	1.1Hz		

3.2   Numerical Dataset

For each bridge state (i.e., BC0 and BCM1:BCM3), the acceleration response of the sensing vehicle's axles is obtained based on the methodology presented in Sect. 2. The response for each axle is only considered for the duration when they are on the bridge. Figure 2 shows an acceleration response sample of both axles at the healthy condition.

To create the dataset of vehicle responses for training the unsupervised data-driven framework, the response of the vehicle's axles traveling over the healthy
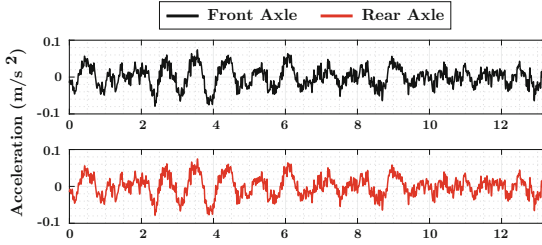
Fig. 2. Illustration of the acceleration time response of the vehicle's front and rear axles while traveling over the healthy state of the bridge.

bridge 500 times is first obtained, and a training-testing ratio of 80:20 is used. Then, 100 responses of the vehicle passing over each damaged bridge conditions are collected for testing. Additionally, random road profiles on each vehicle pass are considered.

4   Bridge Damage Assessment Framework

4.1   Convolutional Variational Autoencoders

CVAE is an adaptation of the Variational Autoencoders (VAE), in which the dense layers are replaced by convolutional layers. It consist of two parts: an encoder and a decoder convolutional neural networks. The first one, reduces the input dimension to a latent space, while the latter attempts to reconstruct the input from the latent variables [21]. Figure 3 shows the structure of the CVAE, where the input corresponds to the continuous wavelet transform (CWT) of the acceleration signal of the vehicle, for the purpose of this work. The encoder CNN encodes the input to a smaller dimension output, used as latent variables z, which are given by the mean, μ, and variance, σ^2, of the probability distribution $q(z|x)$ [21]. x represents the features of the input. The decoder CNN, reconstructs a sample from latent state distribution. The optimization function of the CVAE, is to maximize the Evidence Lower Bound (ELBO) [21].
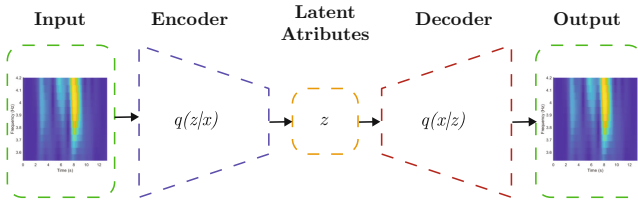

Fig. 3. Structure of CVAE, used as unsupervised anomaly detection algorithm for bridge damage assessment.

The architecture of the CVAE is based on the reference studies [16,21]. The size of the color input images for the CVAE is 224×224. The encoder consists of six convolutional layers, with 3×3 filters, and stride of 2. The output of the encoder has a dimension of 1×1×64, from which the z is obtained. Similarly, the decoder is composed of seven transposed convolutional layers with 3×3 filters and stride of 2. Its output is a reconstructed image with same size as the input of the encoder. Between each convolutional layer in both the encoder and decoder, a Rectified Linear Unit (ReLU) activation function is applied. The hyper-parameters used in the CVAE model are: 100 epochs, batch size of 32 images, and a learning rate of 1×10^{-3}

4.2   Methodology

The methodology for the unsupervised learning framework proposed in this paper is represented by the flowchart in Fig. 4. Additionally, the steps are described next:

1. *Time-Frequency domain analysis:* The residual CWT, C_{red}, is obtained as follows: $C_{res} = C_{front} - C_{rear}$, where C_{front} and C_{rear} are the CWT for each axle's acceleration in the frequency range $3.5Hz$ to $4.2Hz$.
2. *Signal averaging:* The C_{res} from 30 samples are averaged to capture the bridge-related information by nullifying external perturbations.
3. *Training and testing CVAE:* The CVAE presented in Sect. 4.1 is trained with the healthy averaged C_{res}.
4. *Damage index calculation:* The Root Mean Square Error (RMSE) between the original and the reconstructed sample is used as damage index.
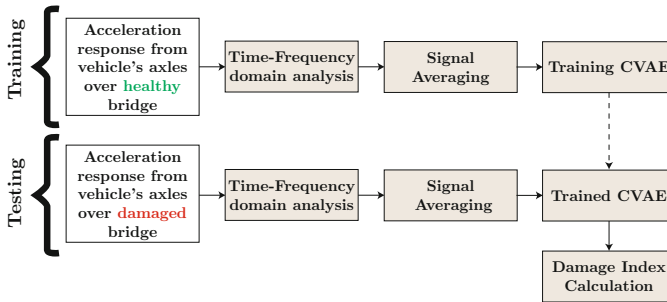
Fig. 4. Flowchart of the unsupervised learning framework for bridge damage assessment.

5   Results

In this section, the proposed framework for bridge damage assessment is implemented. The numerical dataset elaborated in Sect. 3 is used to show the proof of concept of the proposed methodology. Figure 5 presents examples of samples of the CWT for each of the bridge states BC0 and BCM1:BCM3 used in this section to assess bridge damage. Figure 5a presents the CWT of a single acceleration signal from the front axle of the sensing vehicle. Figure 5b presents the C_{res} of single samples, and Fig. 5c shows the averaged C_{res} using 30 samples. It is evident from Fig. 5a that identifying the change in natural frequency from the signal from the front axle is challenging since it is mainly controlled by external factors like the road roughness. However, by obtaining the residual CWT, C_{res}, (see Fig. 5b) the bridge-related information is more evident by observing the frequency peak (i.e., *yellow* color), corresponding to the first natural frequency of the bridge. Further removal of external perturbations like the road roughness can be done by averaging the C_{res} as in Fig. 5c.
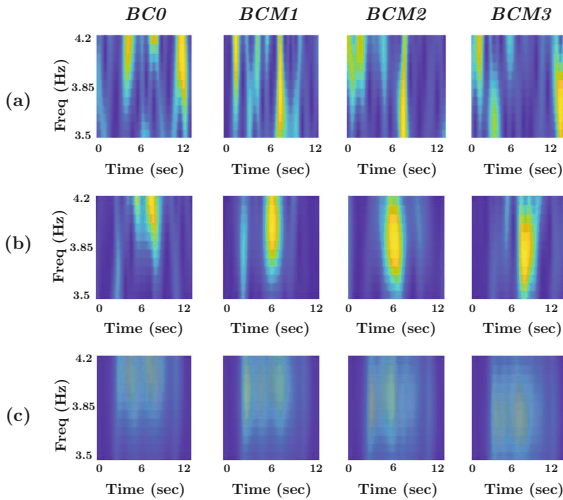
Fig. 5. Examples of CWT of acceleration signals from sensing vehicle's axles used for training and testing the CVAE. (a) CWT of a single acceleration signal from the front axle, (b) C_{res} of single sample, (c) Averaged C_{res}.

Recalling Sect. 3.2, 400 healthy samples are used for training, and 100 from each bridge state are used for testing the CVAE for three different case scenarios. The first one corresponds to training and testing the CVAE with the CWT from the acceleration signals from the front and rear axle of the vehicle (as in Fig. 5a). The second one uses the C_{res} from single samples (as in Fig. 5b), and the third one uses the average of 30 samples of C_{red} (as in Fig. 5c).
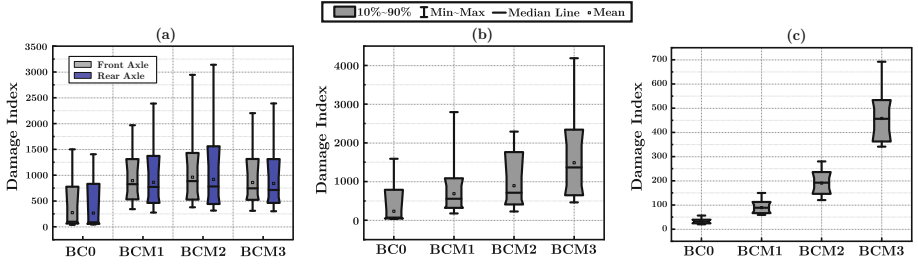
Fig. 6. Box plot of damage indices for multiple bridge states including healthy state, BC0 and damage states of BCM1:BCM3. (a) First case, (b) Second case, (c) Third case.

From the box plots presented in Fig. 6a and b, it is evident that in the first and second scenario, damage can not be identified or quantified, since there is significant overlap between the damage conditions and the healthy condition. The third scenario in Fig. 6c, is not only able to identify the damage, but also it is able to quantify it by having different damage indices for the various bridge states, with no significant overlap between the box plots. As expected, the larger the damage severity, the larger the damage index. These results demonstrate the advantage of utilizing CVAE together with the averaged C_{red}.

6   Conclusions

This paper proposed an unsupervised learning framework using CVAE to identify and quantify damage on simply supported bridges using drive-by inspection technology. A time-frequency domain representation of the recorded acceleration signals from the front and rear axles is used to train and test the proposed methodology. The results showed that the proposed framework is able to identify and quantify different damage conditions of the bridge at mid-span when the average residual CWT from different samples used. In terms of future work, the authors are currently exploring the extension of the framework to bridge damage localization, and its application in real-world context, specifically, on several large-scale bridges located in the state of NSW in Australia.

References

1. Lin, W., Yoda, T.: Bridge Engineering: Classifications, Design Loading, and Analysis Methods. Butterworth-Heinemann (2017)
2. Zhu, X.Q., Law, S.S.: Structural health monitoring based on vehicle-bridge interaction: accomplishments and challenges. Adv. Struct. Eng. **18**(12), 1999–2015 (2015)
3. Sun, L., Shang, Z., Xia, Y., Bhowmick, S., Nagarajaiah, S.: Review of bridge structural health monitoring aided by big data and artificial intelligence: from condition assessment to damage detection. J. Struct. Eng. **146**(5), 04020073 (2020)
4. Mei, Q., Gül, M., Boay, M.: Indirect health monitoring of bridges using Mel-frequency cepstral coefficients and principal component analysis. Mech. Syst. Signal Process. **119**, 523–546 (2019)
5. Wang, Z.L., Yang, J.P., Shi, K., Xu, H., Qiu, F.Q., Yang, Y.B.: Recent advances in researches on vehicle scanning method for bridges. Int. J. Struct. Stab. Dyn. **22**(15), 2230005 (2022)
6. Khan, S.M., Atamturktur, S., Chowdhury, M., Rahman, M.: Integration of structural health monitoring and intelligent transportation systems for bridge condition assessment: current status and future direction. IEEE Trans. Intell. Transp. Syst. **17**(8), 2107–2122 (2016)
7. Yang, Y.B., Chang, K.C.: Extraction of bridge frequencies from the dynamic response of a passing vehicle enhanced by the EMD technique. J. Sound Vib. **322**(4), 718–739 (2009)
8. Yang, Y.B., Chang, K.C.: Extracting the bridge frequencies indirectly from a passing vehicle: parametric study. Eng. Struct. **31**(10), 2448–2459 (2009)
9. Keenahan, J., OBrien, E.J., McGetrick, P.J., Gonzalez, A.: The use of a dynamic truck–trailer drive-by system to monitor bridge damping. Struct. Health Monit. **13**(2), 143–157 (2014)
10. González, A., OBrien, E.J., McGetrick, P.J.: Identification of damping in a bridge using a moving instrumented vehicle. J. Sound Vib. **331**(18), 4115–4131 (2012). https://doi.org/10.1016/j.jsv.2012.04.019
11. Yang, Y.B., Li, Y.C., Chang, K.C.: Constructing the mode shapes of a bridge from a passing vehicle: a theoretical study. Smart Struct. Syst. **13**, 797–819 (2014)
12. McGetrick, P.J., Kim, C.W.: An indirect bridge inspection method incorporating a wavelet-based damage indicator and pattern recognition. In: Proceedings of IX International Conference on Structural Dynamics EURODYN, pp. 2605–2612 (2014)
13. Ju, S.H.: Vibration analysis of 3D timoshenko beams subjected to moving vehicles. J. Eng. Mech. **137**(11), 713–721 (2011)
14. Gkoumas, K., Bono, F., Galassi, M.C., Gkoktsi, K., Tirelli, D.: State of play and challenges for the successful implementation of indirect structural health monitoring (iSHM) for bridges. Bridge Maintenance, Safety, Management, Life-Cycle Sustainability and Innovations. CRC Press (2021). 7 pages
15. Liu, J., Berges, M., Bielak, J., Garrett, J., Kovacevic, J., Noh, H.Y.: A damage localization and quantification algorithm for indirect structural health monitoring of bridges using multi-task learning. AIP Conf. Proc. **2102**, 090003 (2019)
16. Zhang, Y., Xie, X., Li, H., Zhou, B.: An unsupervised tunnel damage identification method based on convolutional variational auto-encoder and wavelet packet analysis. Sensors **22**(6), 2412 (2022)
17. Makki Alamdari, M., Chang, K.C., Kim, C.W., Kildashti, K., Kalhori, H.: Transmissibility performance assessment for drive-by bridge inspection. Eng. Struct. **242**, 112485 (2021)

18. Sinha, J.K., Friswell, M.I., Edwards, S.: Simplified models for the location of cracks in beam structures using measured vibration data. J. Sound Vib. **251**(1), 13–38 (2002)
19. Mechanical Vibration - Road Surface Profiles - Reporting of Measured Data. International Organization for Standardization, Geneva, CH, Standard (2016)
20. McGetrick, P.J., Kim, C.W., González, A., et al.: Dynamic axle force and road profile identification using a moving vehicle. Int. J. Archit. Eng. Constr. **2**(1), 1–16 (2013)
21. Zilvan, V., et al.: Convolutional variational autoencoder-based feature learning for automatic tea clone recognition. J. King Saud Univ. Comput. Inform. Sci. **34**(6), 3332–3342 (2022)